Simulation and optimization of a sub-micron beam for macromolecular crystallography using SHADOW and XOP at GM/CA CAT at the APS

Zunping Liu*, Shenglan Xu, Derek W. Yoder and Robert F. Fischetti**
GM/CA CAT, Biosciences Division, Argonne National Laboratory, Argonne, IL 60439, USA

ABSTRACT

The small, high intensity and low convergence beams available on beamlines at 3rd generation synchrotron sources have been a boon to macromolecular crystallography. It is now becoming routine to solve structures using a beam in the 5 - 20 micron (FWHM) range. However, many problems in structural biology suffer from poor S/N due to small (a few microns) crystals or larger inhomogenous crystals. In additional, theoretical calculations and experimental results have demonstrated that radiation damage may be reduced by using a micron-sized X-ray beam. At GM/CA CAT we are developing a sub-micron, low convergence beam to address these issues. The sub-micron beam capability will be developed on the existing beamline 23ID-D where the minimum beam size available to users is currently 5 microns in diameter. The target goals are a beam size of ~0.8 micron (FWHM) in diameter, with a beam convergence of less 0.6 milli-rads, a flux greater than $5x10^{10}$ photons/sec, and an energy range from 5 to 35 keV. Five optical systems will be compared: 1) a single set of highly demagnifying Kirkpatrick-Baez (K-B) mirrors, 2) multiple Fresnel Zone Plates (FZP), 3) a set of K-B mirrors focusing to a secondary source that is imaged by another set of K-B mirrors, 4) a set of K-B mirrors focusing to a secondary source that is imaged by a FZP, 5) a horizontal focusing mirror focusing to a secondary source that is imaged by another horizontal mirror together with a vertical focusing mirror. Here we will present the results of a design optimization based on ray trace simulations (SHADOW), flux calculations (XOP), and experimental results on 23ID.

Keywords: Sub-micron beamline, ray tracing, optimization, simulation

1. INTRODUCTION

GM/CA CAT mini-beams of 5- 10- and 20-μm diameter have been essential to solving some of the most important crystal structures published in the past three years [1]. Users can rapidly (few seconds) and robustly (without re-alignment) change the beam size among the 5-, 10- and 20-μm mini-beams and the focused full beam (~25 μm x 65 μm) [2]. The ability to make sample-dependent, on-the-fly decisions about beam tailoring is extremely valuable for a large number of crystallographic problems [3,4].

As structural biologists tackle more challenging targets, especially membrane proteins and macromolecular complexes, the crystallization problems become more challenging, and those crystals that are produced are ever smaller or less perfect. Small, intense X-ray beams are required to obtain diffraction data with good signal-to-noise from micro-crystals and to measure good-quality data from the most perfect regions of larger imperfect crystals. The need for a small beam mandates that, for the most difficult problems, it is essential to maximize the brilliance of the beam.

Of the 5- 10- and 20-μm mini-beams now offered to all users at GM/CA CAT, the 10- and 20-μm mini-beams are used extensively and the 5-μm beam much less so. This is due in large part to the lower flux in the 5-μm beam. The 5- 10- and 20-μm mini-beams are created by aperturing the full beam and not by focusing [2]. This approach was chosen because it is robust and was inexpensive, given the stability and hardware on our beamlines when the capability was developed in 2007. If we could focus the beam into 1 μm or 5 μm, smaller beams would be more heavily used and good data could be obtained from a greater number of important and exciting samples.

Looking to the future, experiments [5] indicate a bright future for high-energy micro-beams and micro-crystals. There is a question of what is the minimum size of a macromolecule crystal that can produce useful crystalline diffraction. The very exciting first results from the Linear Coherent Light Source at Stanford demonstrate that sub-micron protein crystals can produce useful diffraction data if illuminated with an intense enough beam [6]. Thus, crystals of dimension 1 μm should be useful with a 1 μm, very intense beam.

* zpliu@anl.gov; phone 1 630 252-1457; fax 1 630 252-0667

**Corresponding author: rfischetti@anl.gov; phone 1 630 252-0660; fax 1 630 252-0667

2. GOALS AND SPECIFICATIONS

GM/CA CAT has built and operates three beamlines located in sector 23 of the APS. Figure 1 shows the layout of the two canted undulator beamlines and the bending magnet beamline. The two ID beamlines have quite similar layouts. The first optical element on each beamline is a cryo-cooled DCM that is vibrationally isolated from the experimental floor. The 1 mrad separation between the two canted undulator sources was insufficient to support two independent macromolecular crystallography endstations. To increase the separation we chose to use two monochromatic, horizontal deflecting mirrors (HDM) to direct the outboard beam further outboard. Both ID beamlines use bimorph mirrors arranged in a Kirkpatrick-Baez geometry (KBM) to provide a beam focused to as small as 20×65 μm^2 at the sample position. The quad-mini-beam collimator positioned just upstream of the sample serves as a scatter guard for the focused beam or can be used to further reduce the beam size to 5, 10, or 20 μm [2].

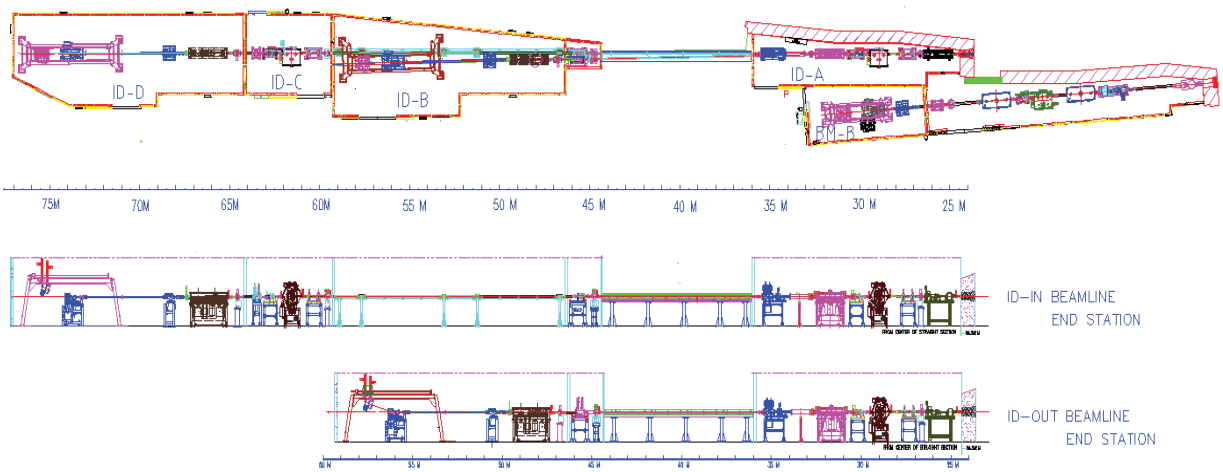

Figure 1. Layout of sector 23 at the APS showing the GM/CA CAT beamlines.

To meet the growing need for even smaller and more intense beams than are achievable with the mini-beam collimator, we plan to rebuild the endstation on 23ID-D. The 23ID-D endstation is at the end of the sector and the lack of a white beam pipe running through it simplifies the design. The beamline is also the longest of the two, which allows a higher demagnification ratio. However, the most important reason is that the fixed angle of incidence HDM mirrors on 23ID-B impose a high energy cut-off of ~20 keV. Beamline 23ID-D can access the higher energies uniquely available in the western hemisphere at the APS as shown in Figure 2. The proposed design will add micro-focusing optics and new goniometry with the goal of delivering a sub-micron beam with high intensity, low convergence/divergence, and high positional stability to a sample on a precision goniometer. The X-ray optical specifications for the new 23ID-D endstation are listed in Table 1.

Table 1. Specifications for the new micro-focus endstation.

PARAMETER	SPECIFICATION
Beam size (FWHM)	minimum < 1.0 μm maximum 10-100 μm
Energy range	6-35 keV with Si(111) and Si(311)
Intensity at focus Si(111)	2×10^{10} photons/sec into 1 μm^2, < 500 μrad^2 at 12.0 keV 5×10^{10} photons/sec into 1 μm^2, < 1000 μrad^2 at 12.0 keV 2×10^{10} photons/sec into 1 μm^2, < 500 μrad^2 at 18.5 keV 5×10^{10} photons/sec into 1 μm^2, < 1000 μrad^2 at 18.5 keV
Positional stability	1/10 beam size over frequency range 1-100 Hz
Intensity stability	1% RMS over frequency range 1-100 Hz

3. OPTICS CONSIDERED

A wide variety of optical components are now available that can provide microfocusing capabilities. These can be divided into broad categories based on the effect used to focus the beam. Diffractive optics include Fresnel Zone Plates (ZP), Multilayer Laue Lenses (MLL) and curved monochromator crystals. Refractive optics include compound refractive lenses (CRL) such as those made from beryllium or kinoform lenses fabricated in silicon. There are also reflective optics such as graded multilayers and

mirrors (mono-bounce-capillaries, toroidial, Montel and KB). An important factor that separates reflective optics from the others is that the focal length is apochromatic, *i.e.*, independent of X-ray energy.

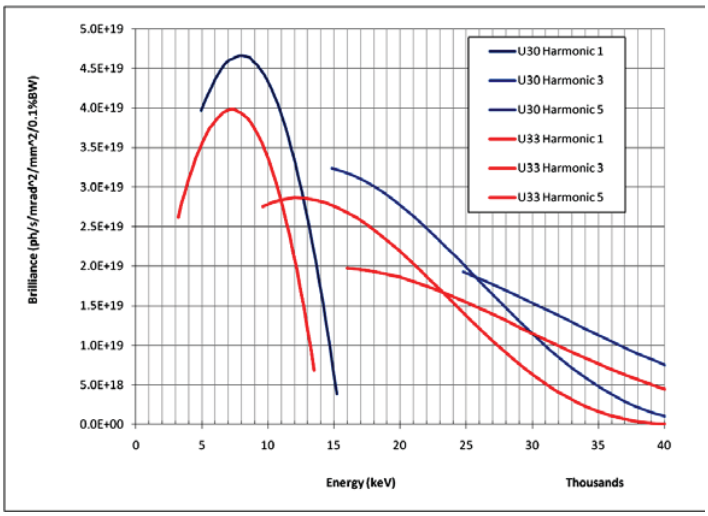

Figure 2. The undulator tuning curves for the two sources at sector 23. Red – the 3.3 cm device (Undulator A) for 23ID-B (ID_{out}). Blue – the 3.0 cm device for 23ID-D (ID_{in}).

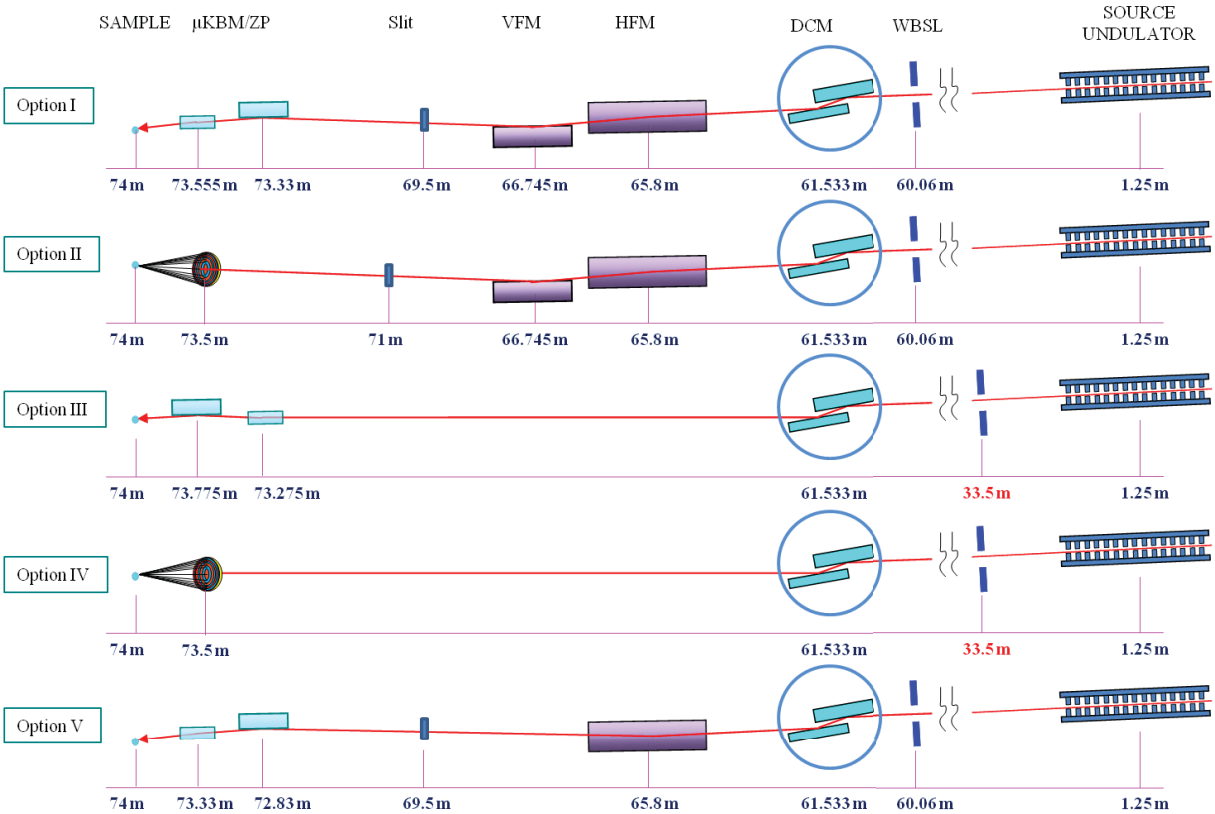

Figure 3. Schematic of Option I-V. For each option there are optical components tagged with corresponding position at beamline.

CRLs have become popular on beamlines that work at a fixed X-ray energy. Implementing them on a beamline with a wide energy range requires inserting an increasing number of lenses into the beam as the energy increases. Since these optics use

refraction, the beam passes through the lens and thus are best used at energies above 15 keV. Similar to ZPs, the beam size at focus would vary with the X-ray energy as the number of lenses is changed.

Kinoform lenses are a special case of CRLs. Compared to some options such as mirror and zone plate optics, kinoform lenses are relatively inexpensive. In principle, these can be constructed to focus in two dimensions, but current lenses provide only one-dimensional focusing. They have the potential to be quite efficient, especially at higher energy where there is less absorption by the lens material. We consider this technology to be in the developmental stage and not ready for implementation on our microfocus beam.

Curved, graded multilayers could be used to focus the monochromatic beam. However, in order to maintain peak reflectivity the angle of incidence must be varied. This would require the endstation to track the beam angle as a function of X-ray energy, and therefore it does not represent a good solution for our micro-focus endstations.

We also explored the option of using a mono-bounce, capillary optic. However, its slope error is large (around 30 μrad), one cannot achieve a 1 μm focus while simultaneously satisfying our intensity and convergence angle specifications.

We conceived nearly a dozen optical designs to achieve a focused 1-μm beam at the sample position, and performed ray-tracing calculations on five design ideas. They are introduced in the following section.

4. RAY TRAYCING SIMULATION

The source is at 1.25 m, DCM at 61.533 m and sample at 74 m at the beamline. The five design ideas use either KB mirrors (KBM), Fresnel zone plate optic (ZP), or combination of KBM and ZP (Fig.3). For example, in Option I the beam is focused by the existing KBM (HFM at 65.8 m and VFM at 66.745 m) to a 2nd source (at 69.5 m) and reimaged with a second set of micro KB mirrors (μKBM with μVFM at 73.33 m and μHFM at 73.555 m) to focus at the sample position. The focal position of the existing KBM ranges from 69.5 m to 72.3 m. Let KBM focus at 69.5 m in order to have larger demagnification for μKBM. It's the same idea for option III and IV to have a new white beam slit (WBSL) at 33.5 m at beamline.

Table 3. The particle beam and X-ray beam source properties.

Particle beam properties		**X-ray beam properties**	
Particle beam energy	7.00	Energy (keV)	12.00
Natural beam emittance, ε	2.50E-09	Intrinsic photon source size, σ_r	1.64
Coupling constant, k_{xy}^2	0.01	Intrinsic photon source divergence, σ_r'	5.02
Horizontal beam size, σ_x	275.00	Photon beam source size, Σ_x	275.00
Vertical beam size, σ_y	9.00	Photon beam source size, Σ_y	12.46
Horizontal beam divergence, σ_x'	11.40	Photon beam source divergence, Σ_x'	9.15
Vertical beam divergence, σ_y'	3.00	Photon beam source divergence, Σ_y'	5.85
Undulator length (end poles omitted)	2.05		
Undulator position relative to center of the straight section	1.25		

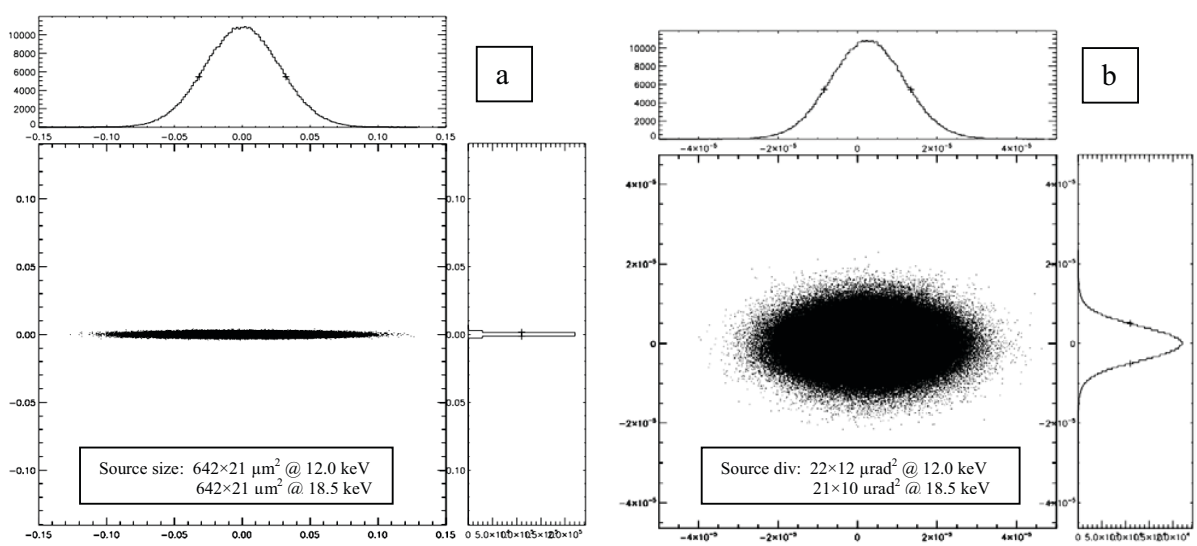

Figure 4. Simulation of the a) source size and b) divergence for 12.0 and 18.5 keV X-rays. The size and angle plots are for 18.5 keV. The numbers on the plot are H×V and FWHM. Note that the standard units used in SHADOW are centimeters.

4.1 Source Property

The program SHADOW was used to simulate the performance of Options I – V. The APS source properties for the APS "low emittance" lattice are summarized in Table 3. The particle beam and undulator parameters (Table 3) were used as input for the source. Figure 4 shows the simulated source size and angular distribution for 12.0 and 18.5 keV X-rays.

XOP is reliable for flux calculation, though it doesn't include effect of electron energy spread [7]. Comparison of flux calculation using XOP, Shadow and SPECTRA has been made. At 18.5 keV, XOP flux (ph/sec/0.1%bw) through a 2.5×1.0 mm^2 slit at 30 m from source of GM/CA-CAT is 2.770E+14, while SPECTRA gives 2.84E+14 (w/o electron energy spread effect) and 2.68E+14 (w/ electron energy spread effect). The XOP flux is used as total rays in simulation to scale beam intensity. At 12 and 16.155 keV, XOP flux through a 2.5×1.0 mm^2 slit at 30 m from source of GM/CA-CAT are 3.366E+14 and 3.185E+14 ph/sec/0.1%bw, respectively.

4.2 Optical systems in Shadow

The optical systems in Shadow are set up according to the schematics of Option-I to V in Figs.3. For example, the optical system for Option-I in Shadow is shown in Fig. 5.

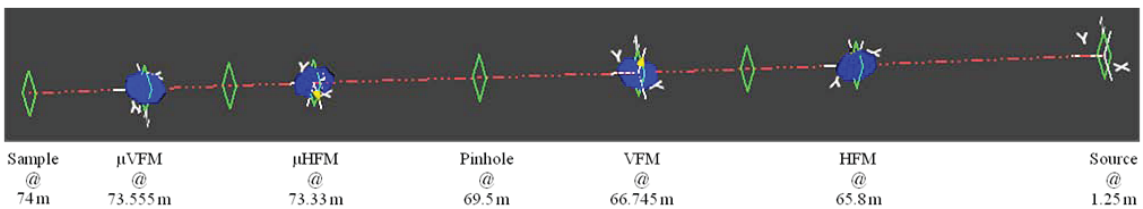

Figure 5. Option-I optical system in Shadow. Axis Y is from upstream to downstream, local X-Z plane of each optical element is perpendicular to Y axis.

The HFM is 1050 mm long with usable optical print length of 1 meter, and the VFM is 600 mm long with usable optical print length of 0.55 meter. Both mirrors have SiO_2, Rh and Pt stripes for harmonics rejection. The Rh stripe is used for simulation for all mirrors. The grazing angle is set as 3 mrad for all mirrors. Therefore, the reflectivity of each mirror would be 94% at 18.5 keV and 95% at 12 keV.

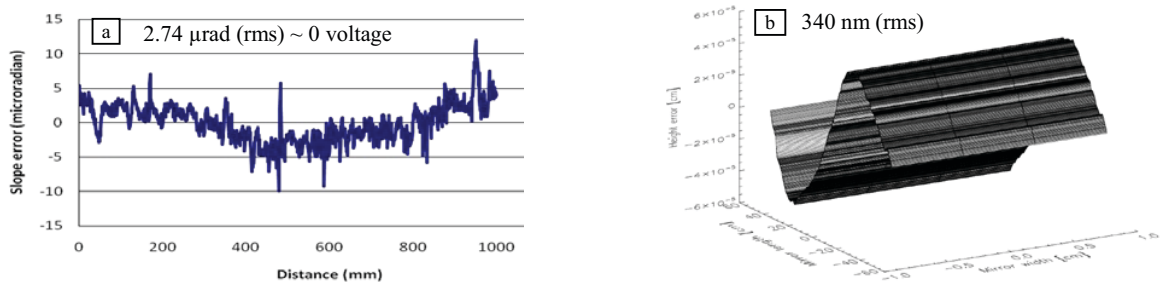

Figure 6. HFM properties for Shadow simulation. a) Slope error 2.74 µrad (rms), corresponding to zero voltage and measured with LTP; and b) shape height error 340 nm (rms) integrated from the LTP slope error.

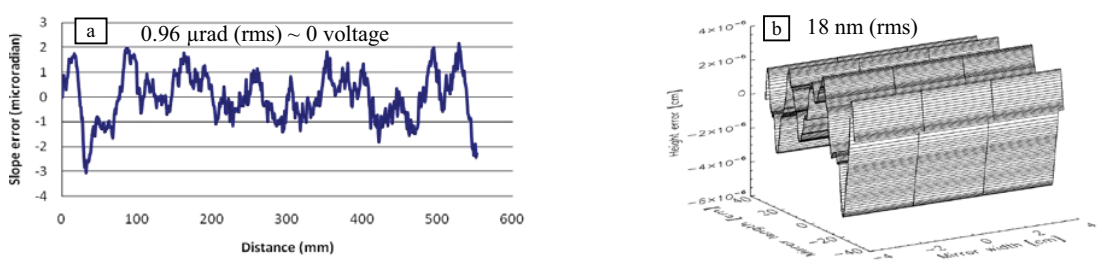

Figure 7. VFM properties for Shadow simulation. a) Slope error 0.96 µrad (rms), corresponding to zero voltage and measured with LTP; and b) shape height error 18 nm (rms) integrated from the LTP slope error.

A KBM's focal spot is strongly affected by slope error [8]. The KBM's shape height error for simulation is generated based on the LTP slope error rather than random wave functions of given value. As shown in Figs. 6-7, the LTP slope error is 2.47 µrad (rms)

for HFM and 0.96 μrad (rms) for VFM, while the shape height error is 340 nm (rms) for HFM and 18 nm (rms) for VFM. For the microfocusing KB mirrors, the slope errors are obtained by scaling VFM's slope error to 0.15 μrad for both μHFM and μVFM. Their shape height errors are also obtained by scaling VFM's. Shadow will take central part of a mirror when its length is shorter than 550 mm.

Ra- tracing of a Fresnel Zone Plate runs through Macros in Shadow [9]. It supposes a ZP is on top of a screen plane and centered on the optical axis. The input parameters are ZP's outer diameter 320 microns, inner zone radius 12.4 microns, focal distance 477.559 mm and nominal wavelength 0.67 Angstrom. The thickness of commercially available ZPs is typically 1600 nm. In order to increase the efficiency a thickness of 3200 nm is required, so that ZP's thickness is taken as 3.2 microns for efficiency calculation.

4.3 Simulation results

The predicted performances for the five layouts are summarized in Table 4 where the mirror length was chosen to maximize the intercepted intensity. However, under these extremes the convergence/divergence specifications were exceeded. Figure 8 shows the focal size and convergence in Option I.

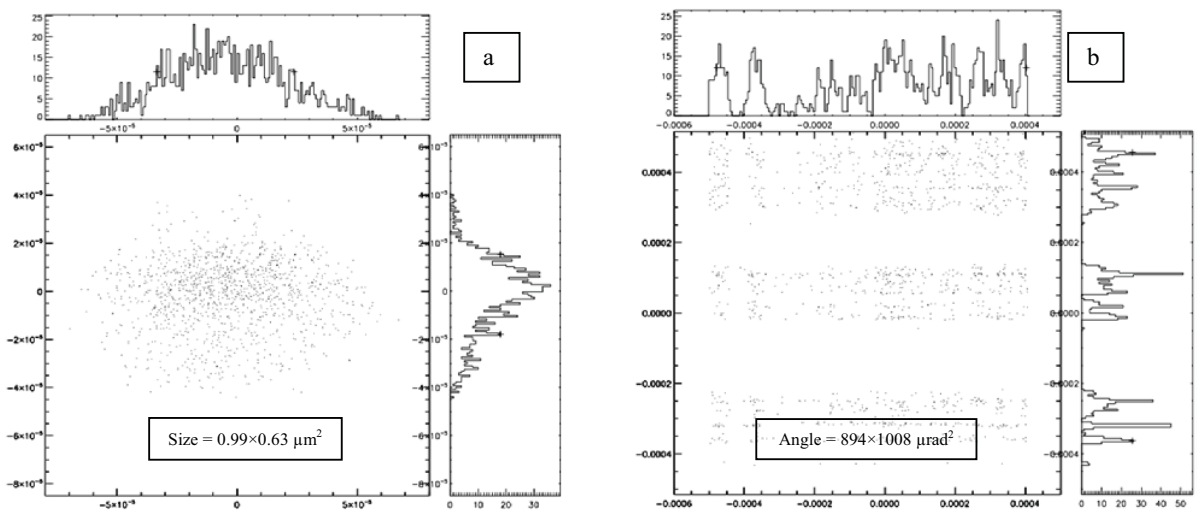

Figure 8. Simulation of the a) focal size and b) divergence at the final focus for Option I. The X-ray energy is 18.5 keV X-rays. The numbers on the plot are H×V and FWHM.

Table 4. Summary performance of Options I-V with mirror length chosen to maximize intensity.

Option	Minimum beam size (μm^2)	Intensity at sample (ph/s)	Convergence (μrad^2)	Mirror length (mm^2)
Option I	0.99×0.63	7.0×10^{10}	900×1000	200×150
Option II	1.2×1.2	2.1×10^{10}	550×550	
Option III	0.89×0.94	6.4×10^{11}	800×600	300×450
Option IV	0.99×0.14	5.0×10^{10}	900×1000	
Option V	0.99×0.89	6.8×10^{11}	1350×600	300×450

Table 5. Summary performance of Options I-V with the added constraint of satisfying the convergence specification.

Option	Minimum beam size (μm^2)	Intensity at sample (ph/s)	Convergence (μrad^2)	Mirror length (mm^2)
Option I	0.99×0.63	2.0×10^{10}	500×500	112×74
Option III	0.89×0.94	2.6×10^{11}	500×500	119×204
Option V	0.99×0.89	1.9×10^{11}	500×500	112×242

In order to also satisfy the convergence/divergence specification the acceptance angle of the mirrors was limited to 500 μrad^2 (Table 5). This results in a loss of intensity and also suggests that shorter mirrors could be used. An important design consideration is whether we should plan to use the longer mirrors providing the highest intensity for demanding experiments, and then use slits just before the mirrors to limit the acceptance angle to reduce the convergence. Alternatively, we could use shorter mirrors, but then not have the ability to open up the acceptance to get more intensity.

4.4 Preferred solutions

The combination of low intensity, variable beam size and the need to realign several components with each energy change make the ZP an undesirable solution for our micro-focus optics. Options I, III and V fit a large number of our design specifications, were studied in greater detail.

Option I has a number of advantages and challenges. We have already tested this concept with a zone plate as the secondary optic and quickly created a focus of 1.23(9) × 1.33(8)μm ^{2}. Furthermore, this geometry seems to be more stable than the other options described below. Of the mirror options, this one (along with Option V) has the lowest cost. The primary challenge is that the estimated final flux will be about an order of magnitude less than the other two mirror solutions. The lower flux results primarily from the need to reduce the working distance (and, in turn, the mirror lengths) to increase the demagnification ratio in order to achieve a sub-micron focus. In addition, this shorter working distance between the most downstream mirror and the sample position creates disadvantages for component positioning within the endstation design.

In Option III the horizontal focus is rapidly changeable, simply by changing the size of the horizontal WBSL. Furthermore, the working distance is greatest for this option. Consequently, the convergence for this option is lower than the others. However, in our experience, such a large separation between the secondary source slit and the ultimate focus leads to greater instability in the focus. In our case, the two are located in different hutches and separated by over 40 m. Additionally, changing the size of the WBSL aperture would drastically change the heat load on the monochromator, introducing further thermal instability into the system. The WBSL aperture may fluctuate under the heat load and introduce intensity noise.

Option V is a hybrid approach that combines aspects of Options I and III. In the vertical direction, the existing vertical KB mirror is removed from the beam path. The new μVFM focuses the storage ring directly in the vertical direction in the same fashion as Option III. This approach provides an order of magnitude greater flux than Option I and slightly more flux than Option III. Also, it does not have the potential thermal instabilities inherent with the WBSL in Option III. In the horizontal direction, this approach is likely to have the same stability that was observed for the geometry of Option I. Option V has a slightly shorter working distance than Option III. In addition, because of the chosen geometry and mirror lengths, this option has the largest horizontal convergence angle (1300 mrad FWHM).

5. OPTIMIZATION

As described above, Option III is in least favor in terms of instability and cost. The slits as secondary source can also help rapidly switch beam size by adjusting slits opening. The solution for Option-I to increase beam flux at focus and working distance while to have desirable focal size and beam convergence is to extend this beamline. The frame that is used to hold the CCD detector could be moved or modified at the downstream end. It is also feasible to extend the back wall of the 23ID-D hutch. The final decision is to extend 1.5 meters for this beamline by extending hutch length. The resultant sample position would be at 75.5 meter, which is 1.5 meters further downstream than before.

Table 6. Summary performance of optimized system setup of Options I & V.

Focal at 75.5m	Option-I				Option-V			
	18.5 keV		12.0 keV		18.5 keV		12.0 keV	
	Reduce Conv	Full Length	Reduce Conv	Full Length	Reduce Conv	Full Length	Reduce Conv	Full Length
size (μm)	0.86×0.50	0.58×0.85	0.59×0.57	0.72×0.95	0.78×0.40	0.81×0.60	0.83× 0.40	0.84×0.61
conv (μrad)	450×412	552×732	441×413	607×767	438×461	609×764	250×469	554×794
flux (ph/s)	4.31E+10	7.13E+10	5.46E+10	1.15E+11	1.74E+11	3.79E+11	1.91E+11	4.10E+11

Extensive studies have been conducted for the trade among beamline performance, dynamics of beam switch, working distance and cost (μKBM length and polishing). In an optimized system setup of Option-I, the secondary source slit has opening 7.7×4.1 μm^2 (H×V), the μVFM sits at 74.58 m and is 300 mm long with usable optical print length of 250 mm, the μHFM sits at 74.88 m and is 200 mm long with usable optical print length of 150 mm. Mirror surface slope errors of μVFM and μHFM take 0.15 μrad. In order to control beam convergence at focal spot, a pair of mono-beam slits (MBSL, 276×433 μm^2 for Option-I and 276×458 μm^2 for Option-V) are put at 74.285 meter. If maximum intensity is preferred, the MBSL would be fully open. The simulation results are summarized at Table 6. The optimized system allows 520 mm working distance while the performance meets the specification in Table 1.

6. DISCUSSION

6.1 Advantage and disadvantage of ray-tracing simulation

When mirror surface slope error in Shadow takes the measured value from LTP, the simulated beam profile is close to true one. Figure 9 shows simulated image at 71.47 m when KBM focus at 69.515 m with or without a Ø4.4 μm pinhole at 69.515. The calculated flux at focus without pinhole is 3.84E+12 ph/sec. Figure 10 shows similar visual images of the same conditions in

experiment. The measured flux without pinhole is 1.7E+12 ph/sec. The ratio of calculated flux to measured result is 2.26, which can be used to scale calculated flux to real one.

Another advantage of ray-tracing with Shadow is that it gives more accurate results than excel estimation when a slit is in beam path. It comes from estimation of the secondary source size in spreadsheet. In Shadow the slit opening is well defined. In excel estimation the opening is treated as full width at half maximum (FWHM), which is over estimated since the small aperture takes beam of maximum near to peak value. Therefore, this estimation leads to larger focal size and more flux. With beam size as design criterion, excel estimation gives conservative results. With beam flux as design criterion, Shadow simulation gives conservative results.

Shadow has trouble to tell what to image when a pinhole is at ray path but it isn't at a focal spot. For example, a pinhole could be put in Option-V between WBSL and μKBM. It could possibly help rapidly switch focal beam size, which Shadow couldn't simulate. Another disadvantage of ray-tracing with Shadow is its speed during extensive study for optimization. In this paper some of optimization process has been speeded up with help from excel estimation, which has been benchmarked with Shadow results.

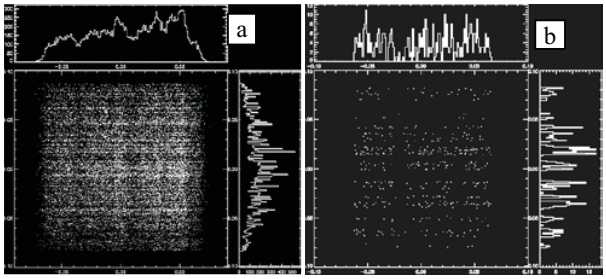

Figure 9. Simulated image of beam off-focus: a) without pinhole and b) with pinhole. At 16.155 kev, KBM focus at 69.515 m, image plane is at 71.470 m. The pinhole Ø4.4 μm sits at KBM focal position. A MBSL 1.5×2.5 mm^2 is right in front of KBM.

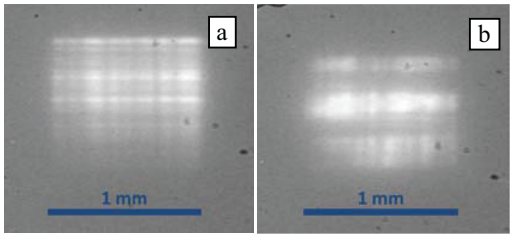

Figure 10. Visual image of beam off-focus: a) without pinhole and b) with pinhole. At 16.155 kev, KBM focus at 69.515±0.050 m, a YAG for image is at 71.470±0.050 m. The pinhole Ø4.4 μm is at KBM focal position. A MBSL 1.5x2.5 mm^2 is right in front of KBM.

6.2 Limitation and expectation

One optimized system setup is given in Section 5. It meets the expected specifications and good working distance. Considering independent elements such as working distance and cost-efficiency, the proposed setup is one of many optimizations. For example, when μKBM take slope error larger than 1.5 μrad for cost purpose, the same system setup will give a larger focal size. But the focal size is going to be larger than 1 μm when the slope error takes 2.2 μrad. With a smaller working distance, a smaller focal size could be made. The proposed optimized system provides a guide line.

7. ACKNOWLEDGEMENT

GM/CA-CAT is funded by the National Cancer Institute (Y1-CO-1020) and the National Institute of General Medical Science (Y1-GM-1104). Use of the Advanced Photon Source was supported by the U.S. Department of Energy, Basic Energy Sciences, Office of Science, under contract No. DE-AC02-06CH11357.

REFERENCES

[1] Rasmussen, S. G. F., *et al*. Crystal structure of the human β_2 adrenergic G-protein-coupled receptor. *Nature* **450**, 383-387 (2007).
[2] Fischetti, R. F., *et al*. Mini-beam collimator enables microcrystallography experiments on standard beamlines. *J. Synchrotron Rad.* **16**, 217-225 (2009).
[3] Sanishvili, R., *et al*. A 7 μm mini-beam improves diffraction data from small or imperfect crystals of macromolecules. *Acta Crystallogr*. **D64**, 425-435 (2008).
[4] Gehret, J. J., *et al*. Terminal alkene formation by the thioesterase of curacin A biosynthesis: Structure of a decarboxylating thioesterase. *J. Biol. Chem*. Epub 27-February (2011).
[5] Sanishvili, R., *et al*. Radiation Damage in protein crystals is reduced with micron-sized X- ray beam. *Proc. Natl Acad. Sci*. E-pub 28-March-2011.
[6] Chapman, H. N., *et al*. Femtosecond X-ray protein nanocrystallography. *Nature* **470**, 73-77 (2011).
[7] Dejus, R. and Sanched del Rio, M., personal communication.
[8] Xu, S. and Fischetti, R.F. A ray-tracing study of the dependence of focal properties on surface figure error for a Kirkpatrick-Baez (K-B) mirror system. SRI: 8th international conference (2004).
[9] Alianelli, L. and Sanched del Rio, M. Shadow example of ray-tracing a Fresnel Zone Plate.